Available online at www.sciencedirect.com
SCIENCE DIRECT®
International Journal of Thermal Sciences 43 (2004) 465–475
International Journal of Thermal Sciences
www.elsevier.com/locate/ijts

Mixed convection in rectangular cavities at various aspect ratios with moving isothermal sidewalls and constant flux heat source on the bottom wall

Guanghong Guo, Muhammad A.R. Sharif *

Aerospace Engineering and Mechanics Department, The University of Alabama, Tuscaloosa, AL 35487-0280, USA

Received 27 January 2003; accepted 21 August 2003

Abstract

Mixed convection heat transfer in a two-dimensional rectangular cavity with constant heat flux from partially heated bottom wall while the isothermal sidewalls are moving in the vertical direction is studied numerically. The enclosure represents a practical system such as an air-cooled electronic device, where cooling from the sides is expected to be an efficient electronic cooling option. The heat source represents a heater or an electronic component located at the bottom in such an enclosure. Several different values of the heat source length, the aspect ratio of the cavity, as well as symmetric and asymmetric placement of the heat source are considered. All computations are done for a range of Richardson number from 0.1 to 10. The influence of the Richardson number, heat source length, placement of the heat source, and aspect ratio of the cavity, on the maximum temperature and the Nusselt number at the heat source surface is investigated. Results are presented in the form of streamline and isotherm plots as well as the variation of the maximum temperature and Nusselt number at the heat source surface under different conditions. The pressure–velocity coupling in the governing equations is achieved using the well-known SIMPLE method for numerical computation. The computational procedure is based on finite volume collocated mesh. The linear algebraic system of equations is solved sequentially using the strongly implicit procedure (SIP).

Keywords: Numerical heat transfer; Rectangular enclosure; Mixed convection; Aspect ratio; Electronic circuit board cooling

1. Introduction

Air-cooling is one of the preferred methods for cooling computer systems and other electronic equipment, due to its simplicity and low cost. It is very important that such cooling systems are designed in the most efficient way and the power requirement for the cooling is minimized. The electronic components are treated as heat sources embedded on flat surfaces [1]. A small fan blows air at low speeds over the heat sources. This gives rise to a situation where the forced convection due to shear driven flow and the natural convection due to buoyancy driven flow are of comparable magnitude and the resulting heat transfer process is categorized as mixed convection. The interaction between buoyancy-driven and shear-driven flows inside a cavity in a mixed convection regime is quite complex.

The problem of convective heat transfer in an enclosure has been studied extensively because of the wide application of such process. Davis and Jones [2] studied the pure natural convection with uniformly heated walls. Papanicolaou and Gopalakrishna [3] simulated the natural convection in a horizontal, enclosed air layer due to a discrete, constant heat flux source at the bottom surface. The parameters studied are the overall aspect ratio (length/height of the layer), the ratio of source length to total length, and the Rayleigh number. Nguyen and Prudhomme [4] studied the free convection flow in a horizontal rectangular cavity submitted to a uniform heat flux at the horizontal as well as vertical walls. Based on the analytical solutions for the flow amplitude in terms of the Rayleigh numbers, the onset and development of convective flow are shown in details.

Mixed convection in enclosures for various different boundary conditions has been studied by Gebhart et al. [5] and Hasanoui et al. [6]. Papaniclaou and Jaluria [7–10] carried out a series of numerical studies to investigate the combined forced and natural convective cooling of heat-

* Corresponding author.
E-mail address: msharif@coe.eng.ua.edu (M.A.R. Sharif).

1290-0729/$ – see front matter
doi:10.1016/j.ijthermalsci.2003.08.008

Nomenclature

A	aspect ratio of the cavity, H/W	Re	Reynolds number
C_p	specific heat of air ..... J·kg^{-1}·K^{-1}	Ri	Richardson number, Gr/Re^2
d	distance from the right edge to the maximum temperature on the heating element ..... m	T	temperature ..... K
d_s	distance of the midpoint of the source plate from the right wall ..... m	U	dimensionless velocity component in horizontal direction
g	gravitational acceleration ..... m·s^{-2}	U_0	magnitude of the sidewall velocity ..... m·s^{-1}
Gr	Grashof number	V	dimensionless velocity component in vertical direction
H	height of the enclosure ..... m	W	width of the enclosure ..... m
k	thermal conductivity of air ..... W·m^{-1}·K^{-1}	α	thermal diffusivity ..... m^2·s^{-1}
L	length of the heat source ..... m	β	thermal expansion coefficient ..... K^{-1}
P	dimensionless local pressure	θ	dimensionless temperature
Pr	Prandtl number	ν	kinematic viscosity ..... m^2·s^{-1}
q''	heat flux at the source ..... W·m^{-2}	ε	dimensionless length of the heat source, L/W

dissipating electronic components, located in rectangular enclosure, and cooled by an external through flow of air. The results indicate that flow patterns generally consist of high- or low-velocity recirculating cells because of buoyancy forces induced by the heat source. Computations for a turbulent flow in mixed convection in a cavity by k–ω model were later performed by Papaniclaou and Jaluria [11]. Numerical solutions were obtained for $Re = 1000$ and 2000 in the range of $Gr = 5 \times 10^7$ to 5×10^8. Iwatsu et al. [12] performed numerical studies for the flow of a viscous thermally stratified fluid in a square container. Shaw [13] investigated three-dimensional mixed convection heat transfer in a cavity heated from below. The influence of Reynolds number and Grashof number on the Nusselt number was discussed. Hsu and Wang [14] investigated the mixed convective heat transfer where the heat source was embedded on a board mounted vertically on the bottom wall at the middle in an enclosure. The cooling airflow enters and exits the enclosure through the openings near the top of the vertical sidewalls. The results show that both the thermal field and the average Nusselt number depend strongly on the governing parameters, position of the heat source, as well as the property of the heat-source-embedded board. Aydin and Yang [15] numerically studied mixed convection heat transfer in a two-dimensional square cavity having an aspect ratio of 1. In their configuration the isothermal sidewalls of the cavity were moving downwards with uniform velocity while the top wall was adiabatic. A symmetrical isothermal heat source was placed at the otherwise adiabatic bottom wall. They investigated the effects of Richardson number and the length of the heat source on the fluid flow and heat transfer.

The present study is based on the configuration of Aydin and Yang [15] where the isothermal heat source at the bottom wall is replaced with a constant flux heat source, which is physically more realistic. The physical model considered here is shown in Fig. 1, along with the important

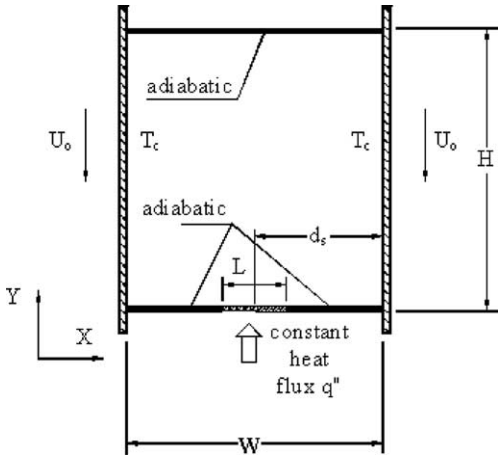

Fig. 1. Schematic diagram of the physical system.

geometric parameters. It consists of a rectangular cavity of dimension, $W \times H$, whose sidewalls are moving downward with a uniform velocity, U_0, and are kept at a constant temperature, T_C. The aspect ratio of the cavity is defined as $A = H/W$. The lower wall has an embedded symmetrical heat source with constant heat flux, q'', and length L. The remaining parts of the bottom wall and the entire upper wall are adiabatic. The enclosure represents a practical system such as an air-cooled electronic device, where the moving sidewalls are an idealization of the cold airflow along the sides of the cavity blown downwards from a fan or a jet at the top. The flow in the cavity is induced by the combined shear force resulting from the movements of the sidewalls and the buoyancy force resulting from the heat source at the bottom wall.

In the present study, the flow and heat transfer phenomena in the cavity are investigated for a series of Richardson numbers and L/W ratios, which is subsequently designated as ε. Asymmetric placement of the heat source, where the heat source is moved towards the right wall is also

investigated. Aydin and Yang [15] did not investigate the effect of aspect ratio on the heat transfer process in the cavity. This study includes additional computations for cavities at various aspect ratios, A, ranging from 0.5 to 2 and their effects on the heat transfer process is analysed and the results are presented in terms of the average Nusselt number and maximum temperature at the heat source surface.

2. Mathematical formulation

The governing equations for laminar steady convection, after invoking the Boussinesq approximation and neglecting the viscous dissipation, can be expressed in the dimensionless form as

$$\frac{\partial U}{\partial X}+\frac{\partial V}{\partial Y}=0 \tag{1}$$

$$U\frac{\partial U}{\partial X}+V\frac{\partial U}{\partial Y}=-\frac{\partial P}{\partial X}+\frac{1}{Re}\left(\frac{\partial^2 U}{\partial X^2}+\frac{\partial^2 U}{\partial Y^2}\right) \tag{2}$$

$$U\frac{\partial V}{\partial X}+V\frac{\partial V}{\partial Y}=-\frac{\partial P}{\partial Y}+\frac{1}{Re}\left(\frac{\partial^2 V}{\partial X^2}+\frac{\partial^2 V}{\partial Y^2}\right)+\frac{Gr}{Re^2}\theta \tag{3}$$

$$U\frac{\partial \theta}{\partial X}+V\frac{\partial \theta}{\partial Y}=\frac{1}{PrRe}\left(\frac{\partial^2 \theta}{\partial X^2}+\frac{\partial^2 \theta}{\partial Y^2}\right) \tag{4}$$

where U and V are the velocity components in the X and Y directions, respectively, P is the pressure, and θ is the temperature. Here, all distances are normalized by W, all velocities are normalized by U_0, and pressure is normalized by ρU_0^2; ρ being the fluid density. The cavity width W is chosen for normalizing the distances since the dimensions H and L are varied while keeping W fixed for varying the aspect ratio, A, and the normalized heat source length, ε. The temperature is normalized as $\theta = (T - T_C)/\Delta T$ where ΔT is the temperature scaling defined as $q''W/k$; k being the thermal conductivity of the fluid. The dimensionless parameters appearing in Eqs. (2)–(4) are the Prandtl number $Pr = \nu/\alpha$, the Reynolds number $Re = U_0 W/\nu$, and the Grashof number $Gr = g\beta\Delta T W^3/\nu^2$, where ν is the kinematic viscosity of the fluid, α is the thermal diffusivity of the fluid, β is the thermal expansion coefficient of the fluid, and g is the gravitational acceleration. The ratio Gr/Re^2 in Eq. (3) is called the Richardson number, Ri, which represents the relative magnitude of the free convection to the forced convection and plays an important role in designating the convection flow regimes. When $Ri \sim 1$ both free and forced convection are equally dominant and the flow regime is designated as mixed convection. If $Ri \gg 1$ then free convection is dominant whereas forced convection is dominant when $Ri \ll 1$. Many of the electronic component cooling processes are operated within mixed convection regime, which is the topic of the present study.

The boundary conditions for the present problem are specified as follows:

Top wall: $\partial\theta/\partial Y = 0,\ U = V = 0$

Bottom wall:

$$\partial\theta/\partial Y = \begin{cases} 0, & \text{for } 0 < X < (1-\varepsilon)/2 \\ -1, & \text{for } (1-\varepsilon)/2 \leqslant X \leqslant (1+\varepsilon)/2 \\ 0, & \text{for } (1+\varepsilon)/2 < X < 1 \end{cases}$$

$U = V = 0$

Right and left wall: $\theta = 0,\ U = 0,\ V = -1$

The condition $\partial\theta/\partial Y = -1$ for $(1-\varepsilon)/2 \leqslant X \leqslant (1+\varepsilon)/2$ at the bottom wall arises as a consequence of constant heat flux q''.

We define the local heat transfer coefficient $h_x = q''/[T_s(x) - T_c]$ at a given point on the heat source surface where $T_s(x)$ is the local temperature on the surface. Accordingly the local Nusselt number and the average or overall Nusselt number can be obtained respectively as

$$Nu = \frac{h_x W}{k} = \frac{1}{\theta_s(X)} \quad \text{and}$$

$$\overline{Nu} = \frac{\bar{h} W}{k} = \frac{1}{\varepsilon}\int_0^{\varepsilon} \frac{1}{\theta_s(X)}\,\mathrm{d}X \tag{5}$$

where $\theta_s(X)$ is the local dimensionless temperature.

3. Numerical procedure

The set of governing equations are integrated over the control volumes, which produces a set of algebraic equations. Central differencing is used to discretize the diffusion terms whereas a blending of upwind and central differencing is used for the convection terms. The convective fluxes at the control volume faces are calculated as $F = F^L + \eta(F^H - F^L)^{\text{old}}$ where the superscripts L and H imply that the fluxes are calculated by the lower order upwind differencing and higher order central differencing schemes, respectively. The value of the blending factor η in the right-hand side ranges between 0 and 1 and the superscript 'old' indicates the value at previous iteration level, which is calculated explicitly and added to the source terms. The source terms in the governing transport equations are not functions of the respective transported variables and are calculated explicitly. The algebraic equations are solved sequentially using the strongly implicit procedure (SIP) proposed by Stone [16]. The pressure–velocity coupling is achieved using the well-known SIMPLE method [17] where the velocity components are first solved using an assumed pressure field (or the pressure field from previous iteration). A pressure correction equation is then solved whose coefficients are functions of the calculated velocity components. The pressure and velocity fields are then corrected based on the pressure correction values. This sequence is repeated until the residuals for all equations are negligible. The computational procedure is based on collocated mesh where the velocity components, pressure, and other scalar variables such as temperature are all stored at the same location (cell center). To avoid the possibility of checkerboard pressure varia-

tion, the mass fluxes across the cell faces are corrected using the pressure gradient across the cell faces. The details of the computational procedure can be found in [18]. The convergence of the sequential iterative solution is achieved when the sum of the absolute differences of the solution variables between two successive iterations falls below a pre-specified small number, which is chosen as 5×10^{-5} in this study.

4. Results and discussion

The FORTRAN computer code of Ferziger and Peric [18] was modified and used for the computations in this study. The working fluid is chosen as air with Prandtl number, $Pr = 0.71$. The normalized length of the constant flux heat source at the bottom wall, ε, was varied to be 0.2, 0.4, 0.6, and 0.8. For each value of ε, computations were performed at $Ri = 0.1$, 0.2, 0.5, 1, 2, 5, and 10 keeping the Reynolds number, Re, fixed at 100.

In order to obtain grid independent solution, a grid refinement study was performed for a square cavity ($A = 1$) at a representative value of $\varepsilon = 0.4$. Fig. 2(a) shows the convergence of the average Nusselt number, $\overline{Nu}$, while Fig. 2(b) shows the convergence of the temperature profile along the vertical mid-plane with grid refinement. It is observed that grid independence is achieved with a 50×50 grid. This grid resolution is therefore used for all subsequent computations for $A \leqslant 1$. For taller cavities with $A > 1$, a proportionately larger number of grids in the vertical direction is used while keeping the number of grids in the horizontal direction fixed at 50.

Due to the lack of experimental data on the particular problem along with its associated boundary conditions investigated in this study, validation of the predictions could not be done against experiment. However, the case of Aydin and Yang [15] with symmetric isothermal heat source at the bottom wall was reproduced. A comparison of the variation of the Nusselt number along the isothermal heat source at the bottom wall and the V velocity components along the horizontal mid-plane, predicted by Aydin and Yang [15] and this study, is shown in Fig. 3 where the agreement is

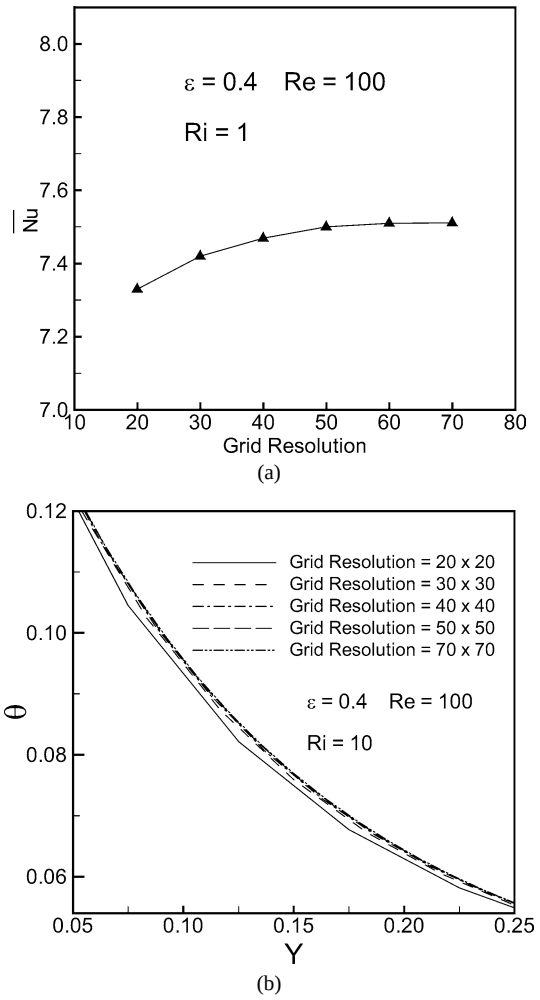

Fig. 2. Convergence of the average Nusselt number and the temperature profile along the vertical mid-plane, with grid refinement.

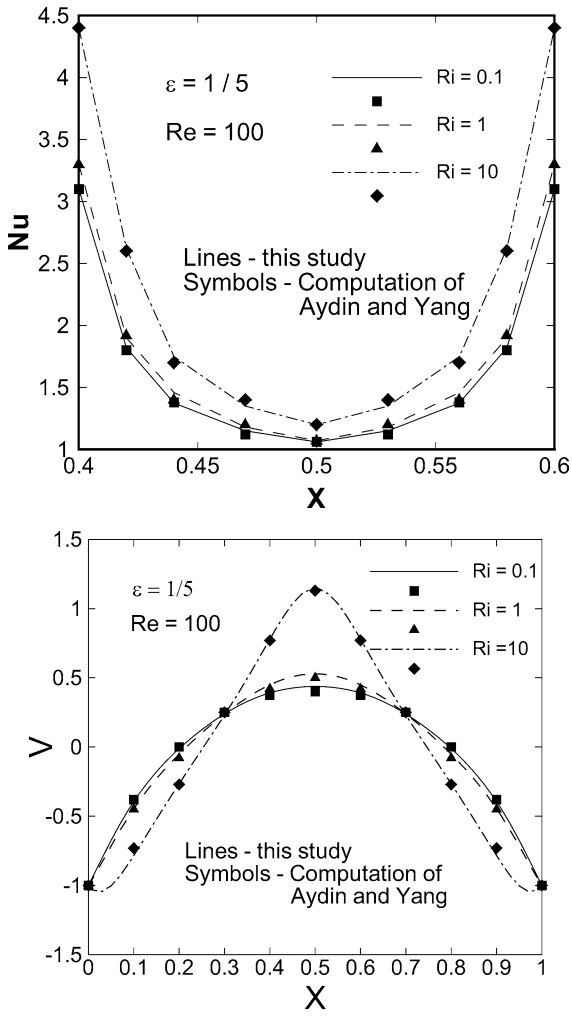

Fig. 3. Comparison of the Nusselt number variation along the isothermal heat source at the bottom and V velocity components along the horizontal mid-plane predicted by the present code with those of Aydin and Yang [15].

found to be excellent. Aydin and Yang [15] validated their result against experimental data. Thus the validity of the present computational process is indirectly established to some extent.

4.1. *Square cavity* ($A = 1$)

The flow and temperature fields in terms of computed streamlines and isotherms for two representative values of the dimensionless source length, $\varepsilon = 0.2$ and 0.6, are shown in Figs. 4 and 5. Plots are shown only for four different values of the mixed convection parameter, $Ri = 0.2$, 1, 5, and 10, for each case. Plots for the whole range of Ri and ε investigated are available in [19].

The solution is symmetric about the vertical midline due to the symmetry of the problem geometry and boundary conditions. In each case the flow descends downwards along the moving sidewalls and turns horizontally to the central region

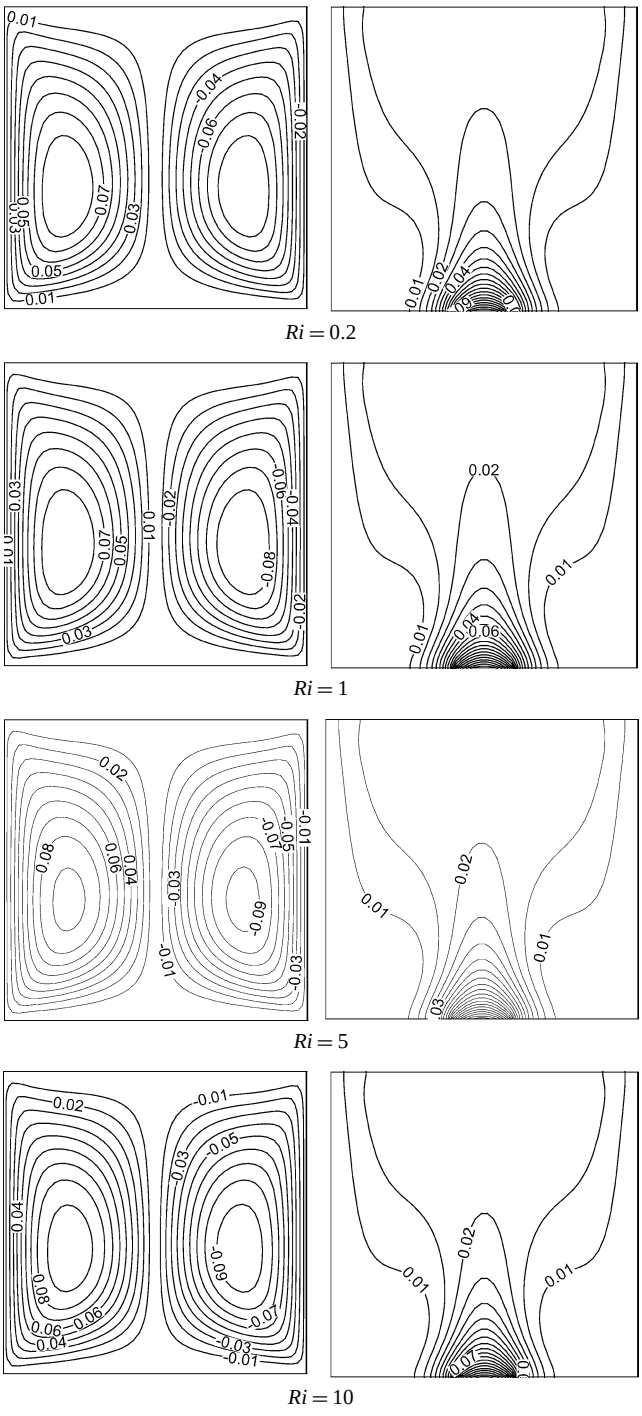

Fig. 4. Streamlines and isotherms for mixed convection case with $\varepsilon = 0.2$.

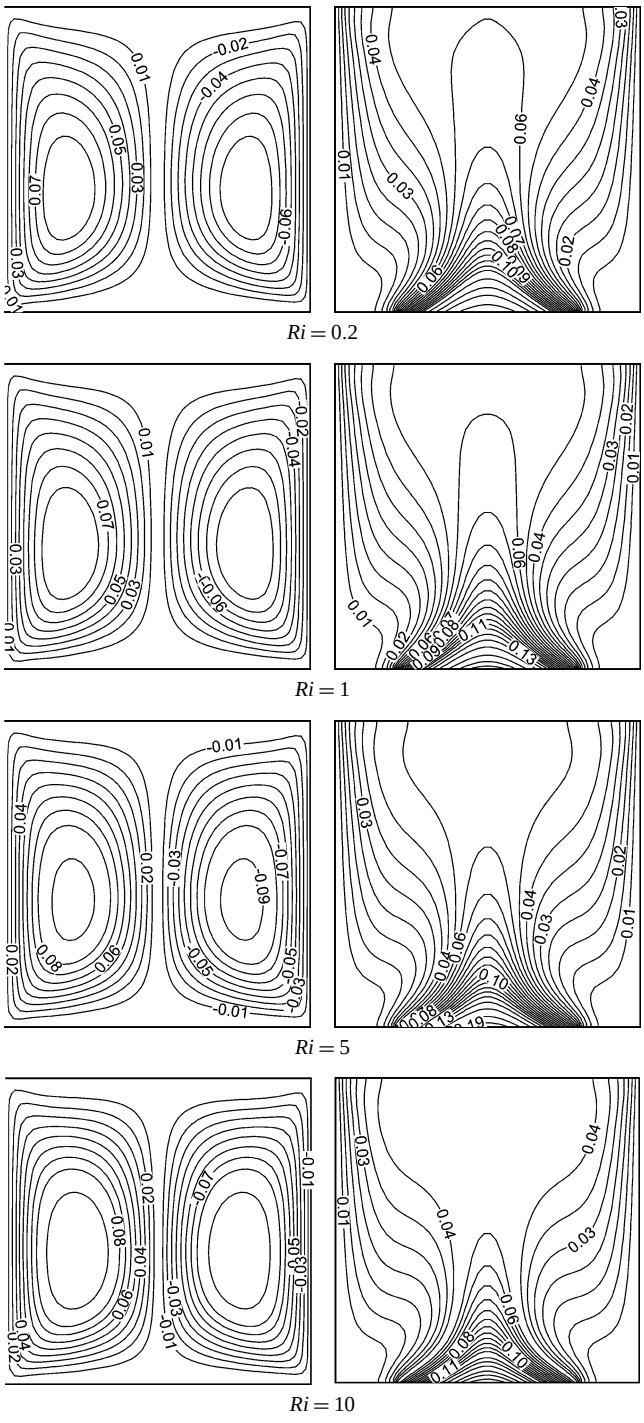

Fig. 5. Streamlines and isotherms for mixed convection case with $\varepsilon = 0.6$.

after hitting the bottom wall. The flow then rises along the vertical symmetry axis and gets blocked at the adiabatic top wall, which turns the flow horizontally towards the cold sidewalls. Thus a pair of counter-rotating rolls is formed in the flow domain. Visual examination of the streamlines does not reveal any significant difference among the different cases. However, noticeable difference is observed in the isotherm plots. The convection region adjacent to the heat source becomes thinner and denser producing higher temperature gradients with increasing *Ri*. Similar behavior is also observed for cases with other values of ε and *Ri* for which the plots are not presented here for brevity.

The mixed convection regime becomes more discernible with the increasing ε because the energy transport increases

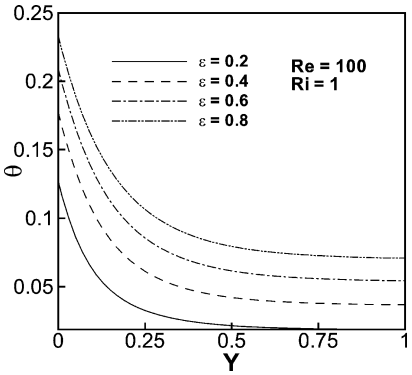

Fig. 6. Temperature profiles along the vertical mid-plane in the cavity.

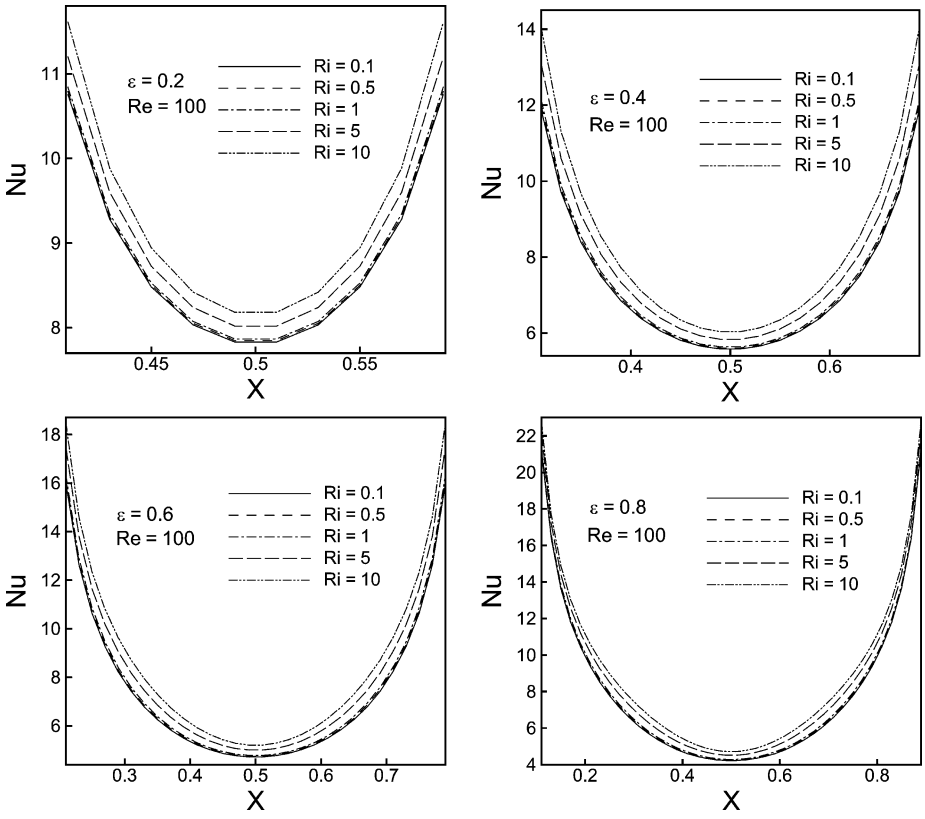

Fig. 7. Variation of the local Nusselt number at the heat source surface.

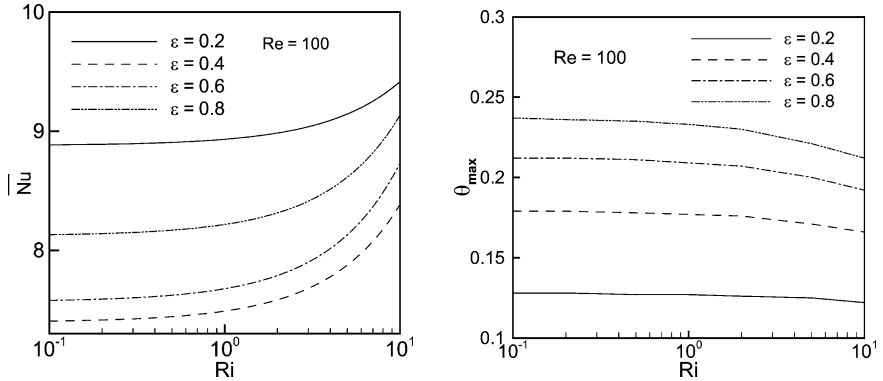

Fig. 8. Variation of the average Nusselt number and maximum surface temperature at the heat source with Richardson number for different heat source length.

due to the increased area of the heated part. Increasing the value of ε makes the range of mixed convection regime larger. Since the isotherm plots change when *Ri* changes, it is the parameter of focus in the analysis for all cases. At low values of *Ri* (< 0.5), the shear force plays the main role in the heat transport. For $Ri \geqslant 0.5$, the buoyancy begins to influence the heat transport and the isotherms with high values tend to concentrate near the heat source surface. This trend keeps on growing as *Ri* increases. When $Ri \geqslant 5$, buoyancy becomes dominant in the heat transfer mechanism and most of the heat transfer phenomenon takes place near the heat source surface. Based on these behaviors, a regime classification for *Ri* can be made as follows: the forced convection regime ($Ri \leqslant 0.2$, with negligible natural convection), mixed convection ($0.5 \leqslant Ri \leqslant 2$, comparable forced and natural convection), and natural convection ($Ri \geqslant 5$, with negligible forced convection).

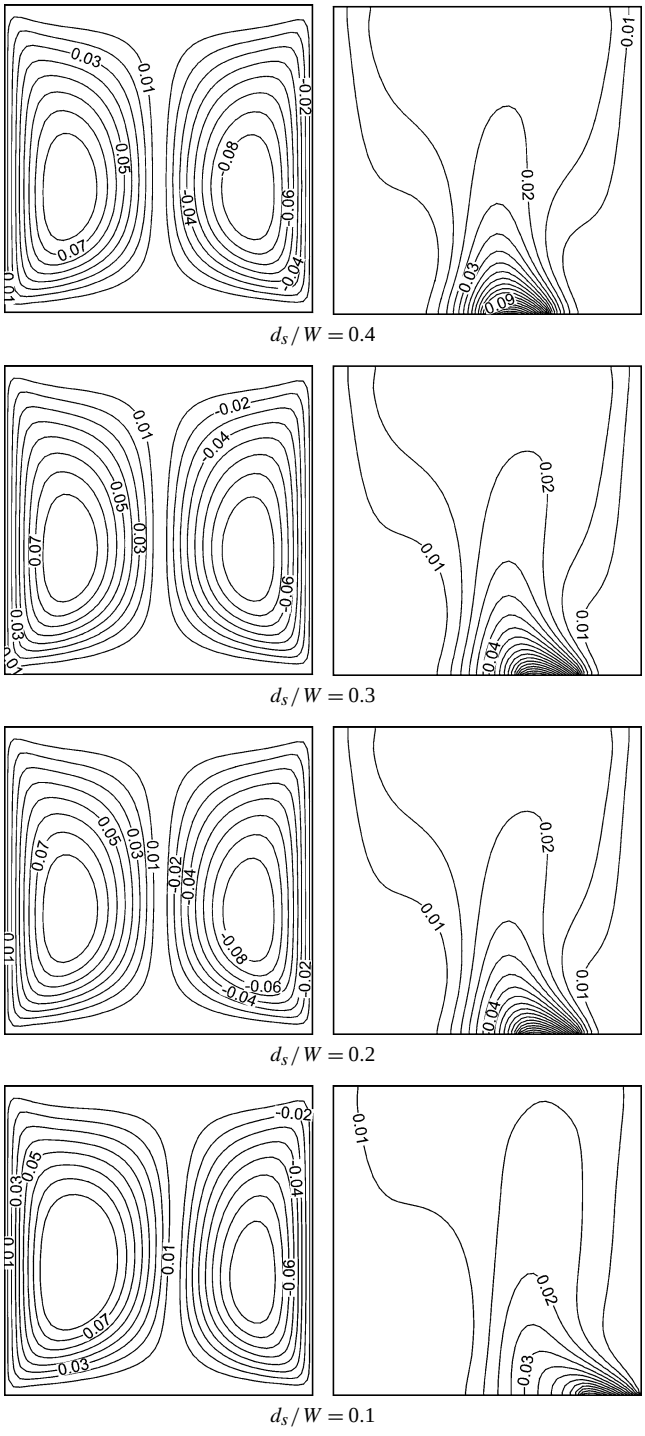

Fig. 9. Streamlines and isotherms for asymmetric placement of the heat source, $\varepsilon = 0.2$, $Ri = 1$, $Re = 100$.

The temperature profiles along the vertical middle section of the cavity for a range of heat source length, ε, at $Ri = 1$ are shown in Fig. 6. It is noticed that the temperature decreases from the bottom to the top along the centreline of the cavity for a particular value of ε. At a fixed height, the temperature increases as the heat source length ε grows. The temperature profiles clearly enunciates the heat transfer behaviour expected from the isotherms given in Figs. 4 and 5, where the most intensive heat transfer region is located near the heat source surface due to the presence of large temperature gradients. The temperature gradients of the cooling air decrease as it ascends from the bottom. When the heat source length ε increases, more heat is transferred into the system, thus the whole temperature level in the cavity is upgraded.

The variation of local Nusselt number, *Nu*, along the heat source surface defined by Eq. (5), is shown in Fig. 7. It is to be noticed in these figures that the length of the heated surface is different for different values of ε. The minimum local *Nu* occurs at the centre of the heat source

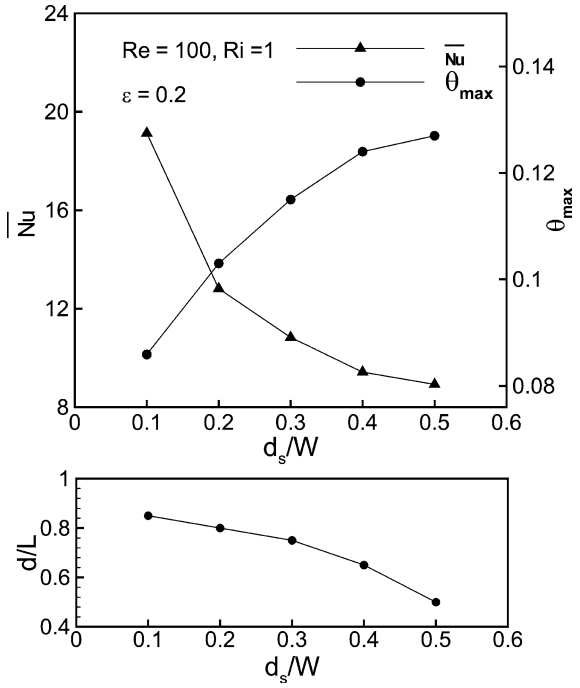

Fig. 10. Effect of the asymmetry of the heating element on the average Nusselt number, $\overline{Nu}$, and the maximum source temperature $\theta_{\max}$ (top). The variation of the normalized distance (d/L) from the right edge of the heating element to the location of $\theta_{\max}$ on the element with d_s/W (bottom).

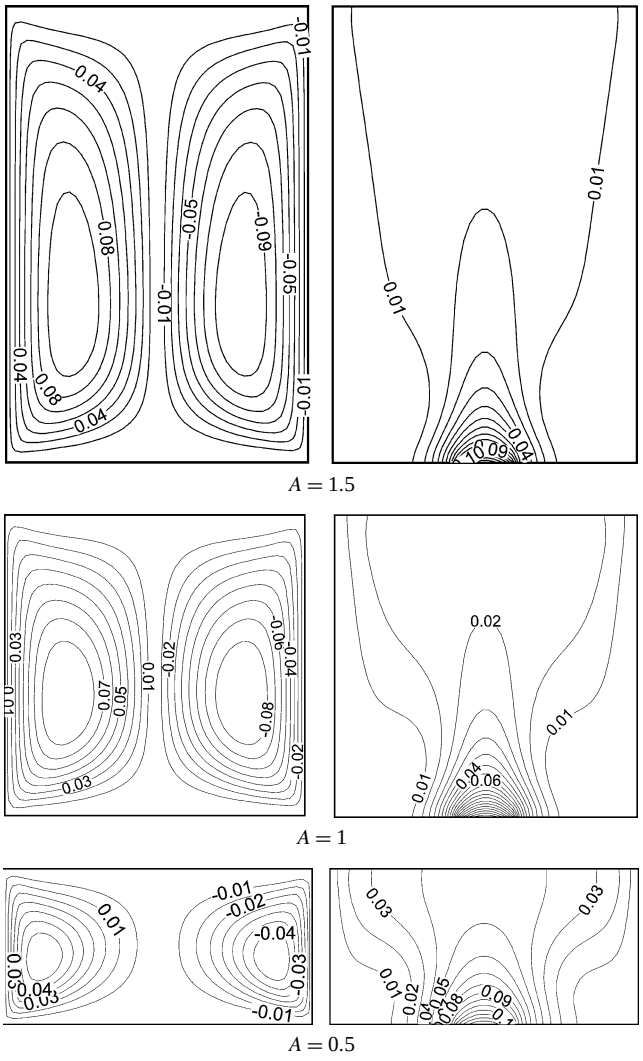

Fig. 11. Streamlines and isotherms for mixed convection case with $\varepsilon = 0.2$ and $Ri = 1$ for different aspect ratios A.

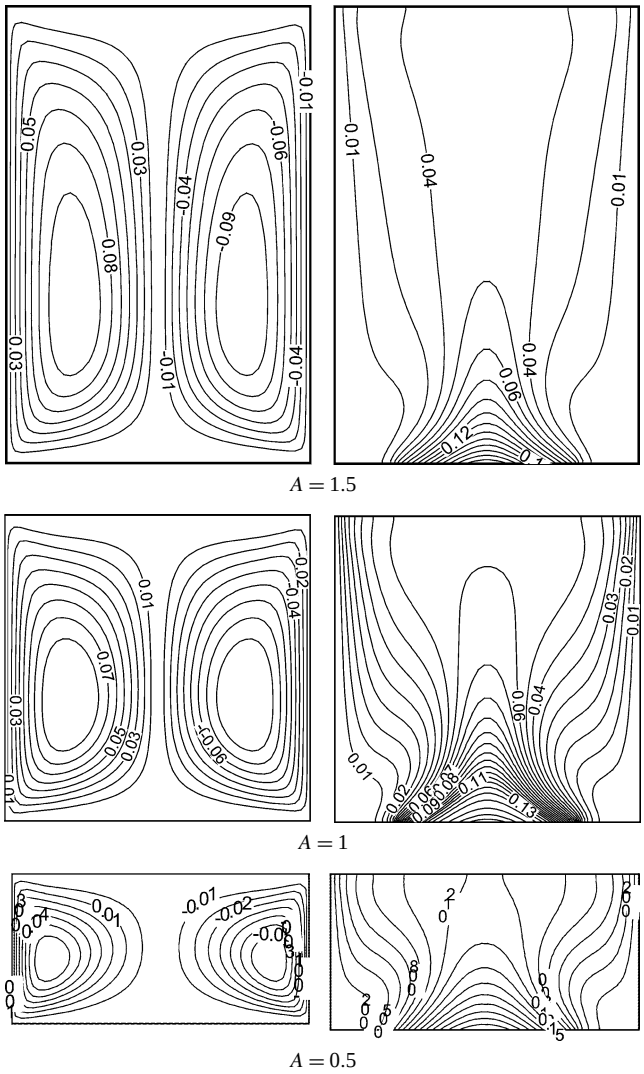

Fig. 12. Streamlines and isotherms for mixed convection case with $\varepsilon = 0.6$ and $Ri = 1$ for different aspect ratios A.

and increases to a maximum at the edge of the heated surface. Due to the symmetrical boundary conditions, two symmetric convection cells are generated and their interface behaves like an insulator. The centre of the heat source surface becomes the stagnation point of the heat transfer area, and attains the maximum temperature and minimum heat transfer rate yielding the minimum Nu.

The variation of the average Nusselt number, $\overline{Nu}$, defined in Eq. (5), against Ri is shown in Fig. 8 for various values of ε. Concentrating on each plot separately for a particular value of ε, a trend of $\overline{Nu}$ increasing with Ri, is observed. When Ri is less than 1, $\overline{Nu}$ grows only slightly with increasing Ri. After Ri is more than 1, $\overline{Nu}$ is found to increase more rapidly. Since Re is kept constant the forced convection effect remains invariant as Ri increases for a particular case. When $Ri > 1$, the natural convection aids more and more in the heat transfer process in addition to the forced convection which results in more rapid increase of $\overline{Nu}$.

An important information desired from this analysis is the identification of the hottest spot on the heat source and obtain the associated maximum temperature at that point so that detrimental conditions for the electronic circuit board can be avoided. The hottest point is obviously at the middle of the heat source surface, which is a stagnation point due to the flow geometry, and the convection mechanism there is very weak compared to the other regions on the surface. The temperature at this point, $\theta_{\max}$, was obtained from the solution and is plotted as a function of Ri for different values of ε in Fig. 8. An increase in ε increases the total heat transferred, which in turn increases the temperature of the heat source. This is why $\theta_{\max}$ increases with increasing ε for any particular Ri. An increase in the value of Ri leads to a decrease in $\theta_{\max}$ for the same ε because natural convection aids more and more in the heat removal process in addition to the forced convection. The variation in $\theta_{\max}$, however, is insignificant for Ri less than 0.1 if the Reynolds number is

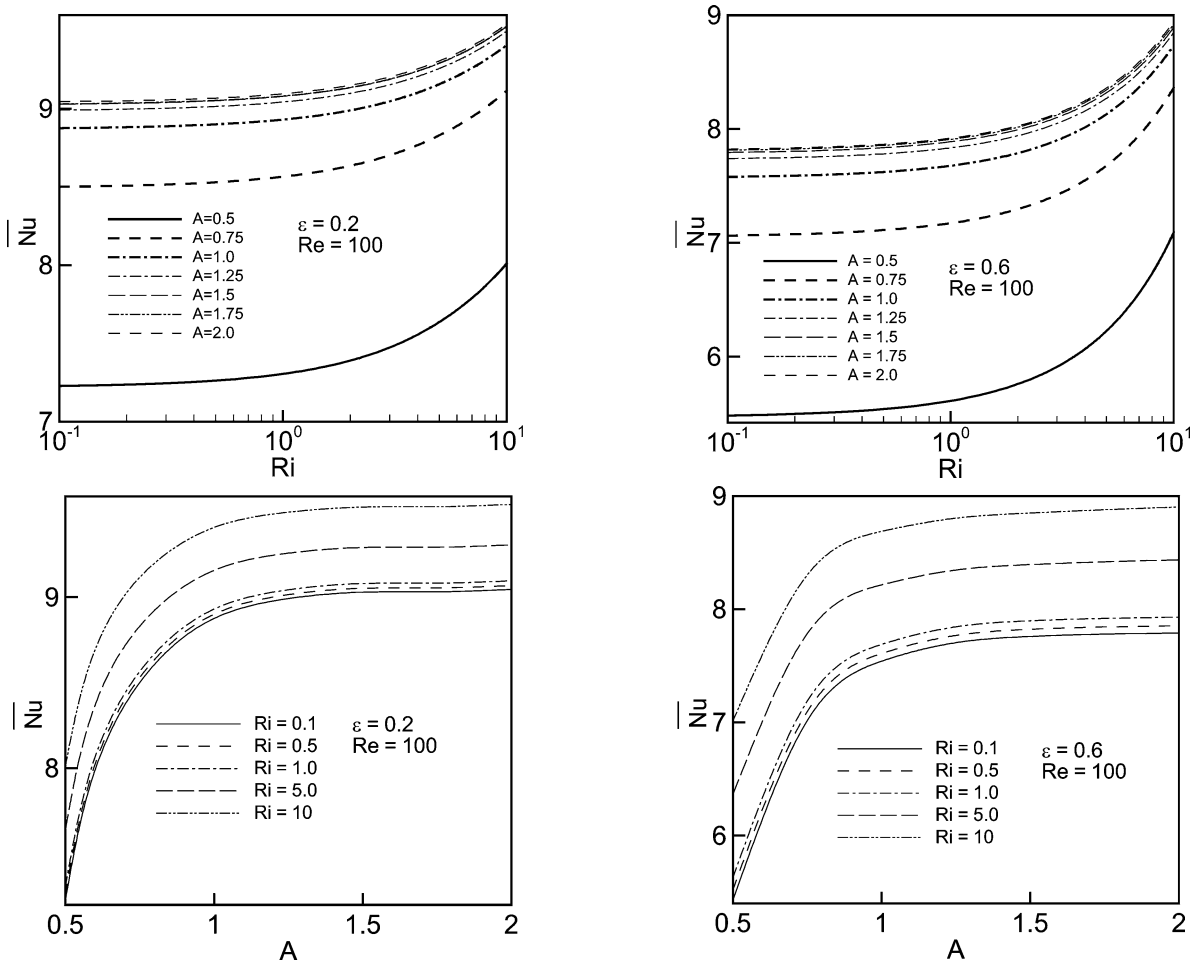

Fig. 13. Variation of the average Nusselt number at the heat source for different Richardson number and aspect ratios.

kept constant. This verifies the earlier assertion that forced convection process dominates for the $Ri \ll 1$ regime.

The analyses presented in the preceding section are for the configuration when the heated surface is placed symmetrically at the bottom. It is also of interest to investigate the effect on the heat transfer for asymmetric placement of the heated surface. For this reason simulations were also performed for such configurations. The characteristic parameter for this configuration is the ratio d_s/W, where d_s is the distance of the mid point of the heated surface from the right wall. For symmetric configuration d_s/W is obviously 0.5. The asymmetric configurations were simulated with d_s/W values of 0.1, 0.2, 0.3, and 0.4. The values of other pertinent parameters such as *Re*, *Ri*, and ε were chosen as 100, 1, and 0.2, respectively.

The predicted flow patterns and isotherms for the asymmetric configurations are shown in Fig. 9. In this case also, two counter-rotating vortices are produced. However, the right hand vortex gets thinner as the d_s/W ratio is decreased. The isotherms also get skewed and move towards the right wall as the d_s/W ratio decreases. Thus the significant part of the heat transfer is occurring through the right hand vortex for the asymmetric configuration.

The maximum temperature, $\theta_{\max}$, and the average Nusselt number, $\overline{Nu}$, at the heat source surface for the asymmetric configuration is obtained from the computed temperature field and is plotted in Fig. 10 as a function of the d_s/W ratio. It is observed that $\theta_{\max}$ increases and $\overline{Nu}$ decreases as the heat source becomes more and more symmetric with increasing d_s/W. In other words, the closer an electronic component is located adjacent to the sidewalls, the better the cooling effect or heat removal is achieved. The normalized distance d/L from the right edge of the heating element to the location of $\theta_{\max}$ on the element for different values of d_s/W is also plotted in Fig. 10. It is noticed that as the heating element is moved towards the right wall, the location of $\theta_{\max}$ moves towards left relative the heating element.

4.2. Rectangular cavities at various aspect ratios

The results presented in the preceding section is for a square cavity for which the aspect ratio, A, is 1. In order to investigate the convective heat transfer behavior at other aspect ratios, computations were also done for cavities at 6 additional aspect ratios of 0.5, 0.75, 1.25, 1.5, 1.75, and 2 with $\varepsilon = 0.2$ and 0.6, keeping *Re* fixed at 100 and *Ri* at 1. The

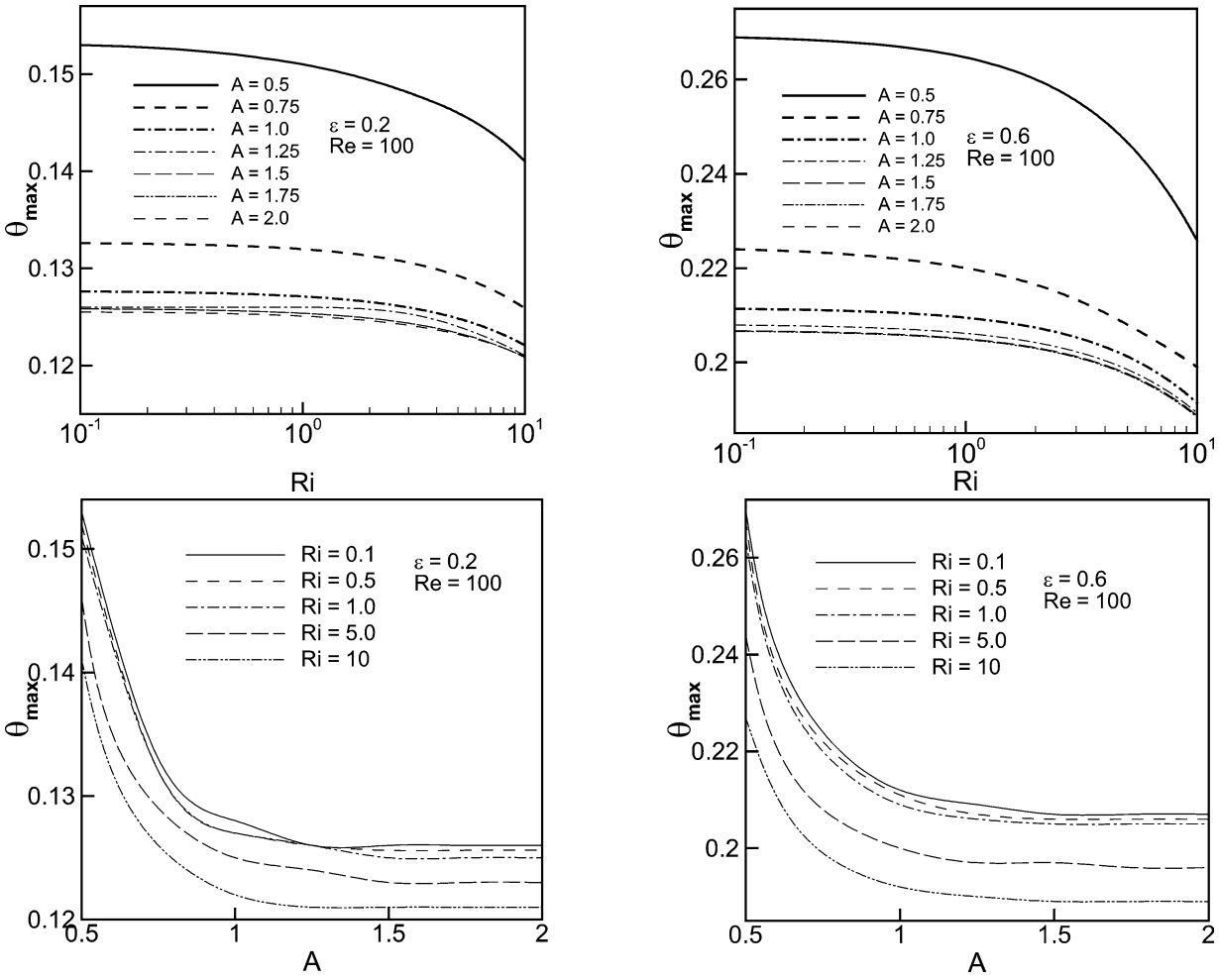

Fig. 14. Variation of the maximum surface temperature at the heat source for different Richardson number and aspect ratios.

flow patterns and temperature fields for $A = 0.5, 1$, and 1.5 as representative cases are compared in Fig. 11 for $\varepsilon = 0.2$ and in Fig. 12 for $\varepsilon = 0.6$. As expected, two counter-rotating vortices are formed at all aspect ratios. However, in the convection region adjacent to the heat source, the isotherms become thinner and denser producing higher temperature gradients (increasing the overall Nusselt number) with increasing A, specially until the cavity changes from thin rectangle to square. This is due to the fact that the cavity volume increases with aspect ratio and more volume of cooling air is involved in cooling the heat source leading to better cooling effect. The average Nusselt number and the maximum surface temperature at the heat source are plotted for a range of Richardson number and aspect ratios in Figs. 13 and 14 from which a trend is observed. For a particular aspect ratio, the average Nusselt number increases while the maximum temperature decreases monotonically with *Ri*. On the other hand, when the Nusselt number and maximum surface temperature are plotted for a particular *Ri* as a function of the aspect ratio, it is observed that the average Nusselt number increases and the maximum surface temperature decreases rapidly with increasing aspect ratio until A is about 1. For $A > 1$ the variation is almost flat indicating that the aspect ratio does not play a dominant role on the heat transfer process at that range.

From these observations, it can be concluded that the overall heat transfer process improves as the aspect ratio increases until the cavity becomes square. For taller cavities $(A > 1)$, the improvement in heat transfer process is not significant.

5. Conclusions

A mathematical model to simulate mixed convective heat transfer in a two-dimensional rectangular enclosure and the associated computer coding has been developed. The model is applied to analyze mixed convection in a square cavity where the cold isothermal vertical sidewalls are moving with constant velocity and a constant flux heat source is placed at the bottom. The moving sidewalls are an idealization of cold air jet blown across the cavity. The cooling airflow caused by the shearing action of the moving sidewalls interacts with the buoyancy-driven flow due to the heat source at the bottom. The resulting processes are investigated to yield quantitative results regarding the cooling effects. The main

parameters of interest are mixed convection parameter, *Ri*, the dimensionless heat source length, ε, and the aspect ratio of the cavity, A. The variation of maximum dimensionless temperature and the average Nusselt number along the surface of the heat source is obtained for a range of *Ri* encompassing the forced, mixed, and natural convection regimes. Symmetric and asymmetric placements of the heat source are considered.

The resulting flow consists of two counter-rotating vortices. As far as the temperature field is concerned, at low values of *Ri*, when forced convection is the dominant mechanism of heat transfer, the temperature is found to be more evenly distributed within the enclosure, and a relatively large region of the enclosure is affected by the heat source. As *Ri* increases and natural convection prevails, the temperature variation is restricted over a gradually diminishing region around the heat source. It is also noticed that the heat-affected region becomes larger with the increasing heat source length.

For asymmetric placement of the heat source, it is observed that the maximum temperature decreases and the average Nusselt number increases as the source is moved more and more towards the sidewall. This is desirable since more effective cooling process is achieved.

For thin rectangular cavities, the heat transfer process improves rapidly as the aspect ratio approaches 1 whereas the improvement is not significant when the cavities are made taller.

References

[1] F.P. Incropera, Convection heat transfer in electronic equipment cooling, J. Heat Transfer 110 (1988) 1097–1111.
[2] G.D. Davis, I.P. Jones, Natural convection in a square cavity: A comparison exercise, Int. J. Numer. Methods Fluids 3 (1983) 227–248.
[3] E. Papanicolaou, S. Gopalakrishna, Natural convection in shallow, horizontal air layers encountered in electronic cooling, J. Electronic Packaging 117 (1995) 307–316.
[4] T.H. Nguyen, M. Prudhomme, Bifurcation of convection flows in a rectangular cavity subjected to uniform heat fluxes, Int. Comm. Heat Mass Transfer 28 (2001) 23–30.
[5] B. Gebhart, Y. Jaluria, R.L. Mahajan, B. Sammakia, Buoyancy Induced Flows and Transport, Hemisphere, New York, 1988, pp. 699–723.
[6] M. Hasnaoui, E. Bilgen, P. Vasseur, Natural convection above an array of open cavities heated from below, AIAA J. Thermophys. Heat Transfer 6 (1990) 255–264.
[7] E. Papanicolaou, Y. Jaluria, Mixed convection from and isolated heat source in a rectangular enclosure, Numer. Heat Transfer, Part A 18 (1990) 427–461.
[8] E. Papanicolaou, Y. Jaluria, Transition to a periodic regime in mixed convection in a square cavity, J. Fluid Mech. 239 (1992) 489–509.
[9] E. Panpanicolaou, Y. Jaluria, Mixed convection from a localized heat source in a cavity with conducting walls: A numerical study, Numer. Heat Transfer, Part A 23 (1993) 463–484.
[10] E. Panpanicolaou, Y. Jaluria, Mixed convection from simulated electronic components at varying relative positions in a cavity, J. Heat Transfer 116 (1994) 960–970.
[11] E. Panpanicolaou, Y. Jaluria, Computation of turbulent flow in mixed convection in a cavity with a localized heat source, J. Heat Transfer 117 (1995) 649–658.
[12] R. Iwatsu, J.M. Hyun, K. Kuwahara, Convection in a differentially-heated square cavity with a torsionally-oscillating lid, Int. J. Heat Mass Transfer 35 (1992) 1069–1076.
[13] H.J. Shaw, Laminar mixed convection heat transfer in three-dimensional horizontal channel with a heated bottom, Numer. Heat Transfer, Part A 23 (1993) 445–461.
[14] T.H. Hsu, S.G. Wang, Mixed convection in a rectangular enclosure with discrete heat sources, Numer. Heat Transfer, Part A 38 (2000) 627–652.
[15] O. Aydin, W.J. Yang, Mixed convection in cavities with a locally heated lower wall and moving sidewalls, Numer. Heat Transfer, Part A 37 (2000) 695–710.
[16] H.L. Stone, Iterative solution of implicit approximations of multi-dimensional partial differential equations, SIAM J. Numer. Anal. 5 (1968) 530–558.
[17] S.V. Patankar, Numerical Heat Transfer and Fluid Flow, Hemisphere, 1980.
[18] J.H. Ferziger, M. Peric, Computational Methods for Fluid Dynamics, Springer, Germany, 1997.
[19] G. Guo, Mixed convection in rectangular cavities with moving sidewalls and partially heated constant heat flux bottom wall, MSc thesis, The University of Alabama, Tuscaloosa, Alabama, 2001.